Effect of Agglomeration on Pulverized-Coal Combustion

ROD W. SHAMPINE,* RUBEN D. COHEN, YILDIZ BAYAZITOGLU, and CLAY F. ANDERSON

Department of Mechanical Engineering and Materials Science, Rice University, Houston, TX 77251, USA

The effect of coal particle agglomeration during pulverized coal combustion is studied using a plug-flow model of a practical coal combustor. The model incorporates turbulent agglomeration, in addition to the combustion equations, to explore certain combustor and coal parameters that may be used for optimizing a chosen output parameter (e.g., burnout time). This routine has been used to develop relations describing the effects of turbulent agglomeration on pulverized coal combustion as an aid in combustor design or retrofitting. The results of this work indicate that, in agreement with general observations, agglomeration will have little impact on pulverized coal combustion in typical combustors.

NOMENCLATURE

A_0	initial ash mass fraction
c_f	turbulent friction coefficient
$\mathscr{D}$	Stokes-Einstein diffusion coefficient, m^2/s
$\mathscr{D}_{O_2}$	diffusion coefficient of oxygen in air, m^2/s
D_P	particle diameter, m
D_c	combustor characteristic diameter, m
f	number of fragments per particle
k	Boltzman constant 1.381×10^{-23} J/K
M_c	molar mass of carbon, 0.012011 kg/mol
M_{O_2}	molar mass of oxygen, 0.031998 kg/mol
n	Rosin–Rammler parameter
P_g	air pressure, Pa
q	mass flux of carbon per unit area, kg/m^2s
R_g	ideal gas constant, 8.314 J/mol · K
SR	stoichiometric ratio
$\tilde{t}$	characteristic time, s
t_b	combustion time with coagulation, s
t_{b0}	combustion time without coagulation, s
T	temperature, K
u_*	turbulent friction velocity, m/s
U	velocity, m/s
x'	Rosin–Rammler parameter, m
X_{O_2}	oxygen mole fraction

Greek Symbols

α	collision efficiency
ϵ	energy dissipation rate, W/s
Γ	shear rate, 1/s
η	number density, $1/m^3$
η_0	bulk number density, $1/m^3$
ϕ	volume fraction of solids
λ	Kolmogorov length scale, m
ρ	density, kg/m^3
τ	Kolmogorov time scale, s
ν	kinematic viscosity, m^2/s

Subscripts

b	burnout
D	diffusion
s	shear
P	particle
T	turbulent
g	gas
m	mean

INTRODUCTION

This paper deals with simultaneous aggregation and combustion in pulverized coal combustion, a phenomenon not treated before. The theory of agglomeration, begun by Smoluchowski [1] in 1917, has been applied in many fields, ranging from powder processing in materials science to particulate-caused pollution in environmental studies. An excellent overview of this subject is presented by Gregory [2], and more detail can be found in Refs. [3–7].

Although works on coal combustion have, in general, neglected the effects of particle agglomeration [8–13, to name a few], fragmenta-

*Corresponding author.

COMBUSTION AND FLAME 101: 185–191 (1995)

Published by Elsevier Science Inc.

0010-2180/95/$9.50
SSDI 0010-2180(94)00192-U

tion of coal-water slurry droplets [14, 15], and agglomeration in fouling [16–18] and soot formation [19–22] have already been looked at. Despite this lack of attention in the literature to aggregation in pulverized coal combustion, an order of magnitude analysis reveals that at certain regions of operating Reynolds number, agglomeration could have a considerable impact in a typical utility combustor employing pulverized coal.

AGGLOMERATION ANALYSIS

Agglomeration is the process in which the number of discrete particles in a system is reduced as smaller particles join together to produce larger ones. The phenomenon is most commonly seen when dealing with particles well under 1 mm in size. Typical examples are found in rain, blood clotting, pollution condensation and fallout, and milk curdling. Applications include water treatment, food and powder processing, separation, and pollution control.

The rate of agglomeration of particles dispersed in a suspending fluid depends on the size of the particles, the degree of mixing, and the charge on the particles. Because modern pulverized-coal utility plants use very finely divided coal and highly turbulent mixing, both of which promote high agglomeration rates, the possibility of agglomeration is worth considering.

Agglomeration can be caused by three mechanisms, each of which can determine the actual rate at which particles collide. These are Brownian diffusion (perikinetic), fluid motion (orthokinetic), and differential settling or drag [2–7].

Brownian motion is the random movement of particles in suspension due to the thermal energy of the system. This motion gives rise to collisions between particles. Velocity gradients in a fluid, induced by shear and turbulent flows, also give rise to collisions as particles moving at different speeds come into contact with each other. Finally, differential settling produces collisions as larger particles overtake smaller ones. This last mechanism, however, is negligible in coal consequence in coal combustors, as even the largest particles are moving at 90%–97% of the bulk velocity and, thus, are not allowed to settle. In order to determine if either perikinetic or orthokinetic agglomeration is important, estimates of the corresponding agglomeration rates are required.

The basic theories of agglomeration are built around three assumptions: (i) particles always stick when they collide (which can be relaxed using the collision efficiency, α); (ii) collisions are binary, involving two particles (or aggregates); and (iii) the process is statistically steady state. The expression for the number density of particles undergoing Brownian agglomeration is [2]

$$\eta(t) = \frac{\eta_0}{1 + t/\bar{t}_D}, \tag{1}$$

where

$$\bar{t}_D \equiv \frac{3kT\eta_0}{4\alpha\mu} = \frac{1}{4\pi\alpha D_p \mathscr{D}\eta_0}. \tag{2}$$

The agglomeration time $\bar{t}_D$ is analogous with the radioactive half-life, since in one period $\bar{t}_D$ the number density of single particles is halved.

In shear-induced agglomeration the number density will exhibit an exponential decay of the form [3]

$$\eta(t) = \eta_0 e^{(-t/\bar{t}_s)}, \tag{3}$$

where the shear agglomeration time, $\bar{t}_s$, is

$$\bar{t}_s = \frac{\pi}{4\alpha\Gamma\phi}. \tag{4}$$

The collision rate β_{12} between particles of any two sizes undergoing shear agglomeration is

$$\beta_{12} = \frac{4}{3}\Gamma\eta_1\eta_2(R_1 + R_2)^3. \tag{5}$$

For identical particles, this result must be divided by 2, to prevent counting each particle twice, once as a test particle, and once as a colliding particle;

$$\beta_{11} = \frac{16}{3}\Gamma\eta_1^2 R_1^3. \tag{6}$$

To apply these two theories to turbulent flow, appropriate length and time scales are required. For isotropic turbulence, these are

the Kolmogorov length and time scales, λ and τ respectively, representing the diameter of the smallest turbulent eddy and its period of rotation.

As suggested by Camp and Stein [24], one may incorporate the Kolmogorov rate $(1/\tau)$ as the shear rate in order to obtain the agglomeration rate in isotropic turbulence. Prior to doing so, however, it is necessary to define the turbulent energy dissipation rate, ϵ, which, along with the kinematic viscosity ν, provides expressions for λ and τ. A dimensional analysis is conjunction with Eq. 4 yields

$$\bar{t}_T = \frac{\pi}{4\phi}\sqrt{\frac{\nu}{\epsilon}}, \tag{7}$$

where $\bar{t}_T$ is the turbulent agglomeration time, and

$$\epsilon = \frac{4u_*^3}{D}, \tag{8}$$

based on experimental work on pipe flow [25]. Here D is the pipe diameter. u_*, the friction velocity, is found from [26]

$$u_* = U\sqrt{\frac{c_f}{8}}, \tag{9}$$

where c_f, the turbulent friction coefficient, is given by [26]

$$c_f = \frac{0.316}{\mathrm{Re}^{1/4}} \tag{10}$$

and $\mathrm{Re} = UD/\nu$.

In order to model diffusive agglomeration in turbulent flow, the diffusivity in equation (2) is corrected to the turbulent diffusivity $\mathscr{D}_T$. From Schlichting [26], therefore,

$$\mathscr{D}_T \approx 0.037UL \tag{11}$$

for a jet of fluid leaving a nozzle of diameter of diameter L and velocity U.

To determine the dominant agglomeration mechanism, it is necessary to compare the particle size, D_p, to the Kolmogorov microscale, λ. For $D_p/\lambda < 1$ agglomeration is dominated by the turbulent shear mechanism [27]. Whereas for $D_p/\lambda > 1$, turbulent diffusion is the controlling mechanism. Finally, if $D_p/\lambda \approx 1$, both mechanisms apply.

With typical values of $\nu \approx 2.07 \times 10^{-4}$ m^2/s, $\eta_0 \approx 10^9$ particles/m^3, $\phi \approx 10^{-5}$, and others listed in Table 1, we find shear agglomeration to be the dominant mechanism, with a characteristic time of $\bar{t}_T = 25$–265 s. Thus, with a residence time scale of around one second, which is typical of a utility coal combustor [8, 9, 12, 13, 28, 29], the effect of agglomeration is indeed small. What follows next is a detailed evaluation of this effect.

COMBUSTION ANALYSIS

Combustion of pulverized coal occurs in two stages: (i) devolatilization and (ii) char combustion. Devolatilization occurs when particles entering the combustor are rapidly heated. Heating rates are 10^4 K/s or higher. With such high heating rates, the volatile material is removed and burned within about 0.02 s. For our purposes, this is sufficiently rapid to be considered instantaneous. With coal composition and volatile content known, the heat evolved and the oxygen consumed can be calculated. This loss of material, which will alter the density and ash content of the resulting char, may be evaluated with the R-factor of Badzioch and Gregory [30]. Anthracite coal was selected (from Ref. 9) for use in the model, with 9.34% volatiles, 26.15% ash, and 4.03% moisture, with the balance carbon. Its initial density is 1636 kg/m^3 with an R-factor of 0. In order to keep the model tractable, we assume that the carbon and oxygen to carbon monoxide reaction is dominant [8].

TABLE 1

Typical Flow Properties of Cement Kilns and Shell Boilers

	Cement Kiln	Shell Boiler
D_c (m)	2.5–3.5	0.75–1.33
Re_{D_c}	1.5–2×10^5	2–5×10^4
U (m/s)	21.6–72	10.8–48
c_f	0.0161–0.0149	0.0266–0.0211
u_* (m)	0.969–3.107	0.623–2.46
ϵ (φ/σ)	1.04–48.0	0.726–79.9
λ (m)	0.0017–0.0007	0.0019–0.0006
D_p (μm)	50	50
D_p/λ	0.0288–0.0751	0.0263–0.0853

The results of Jia et al. [9] also indicate that particle breakup on heating is important for coal particles larger than about 2 mm. Baxter [3], however, provides results for small particles, indicating that the number of daughter particles, measured after combustion, varies with initial particle size and coal rank, and can reach into the hundreds. Both fragmentation during devolatilization and percolate fragmentation (during combustion) are modeled by assuming that the breakup process occurs immediately, and that it produces a number of daughters from each initial particle equal to f. This will cause the model to slightly overpredict the effect of agglomeration due to particles produced by percolate fragmentation. This method was chosen because of a lack of a standard model for percolate fragmentation rates. Anthracite coal can be expected to have an f near one.

COMBINED COMBUSTION AND AGGLOMERATION MODEL

To assess the effect of agglomeration, a plug-flow model of a pulverized coal combustor has been developed. It takes the problem's physical parameters and, using certain assumptions, provides the particle diameter, temperature, and number density histories. These data are then used to calculate "burnout" which is defined as when 99% of the combustible matter is consumed. The solution is accomplished with the IMSL™ routine DIVPRK, a 5th and 6th order Runge–Kutta–Verner method [32].

The model works from 12 physical parameters and 2 mathematical ones. To simplify entry, they are read from a file. The selection of coal type sets the three coal parameters; volatile fraction, ash fraction, and density. The fineness and size distribution is set with the Rosin–Rammler parameters x' and n, which are discussed shortly. Combustor parameters are coal and air feed rates, coal inlet temperature, gas and wall temperature, and inlet diameter. Finally a value for the collision efficiency is needed. The numerical routine further requires values for its time step and the tolerance for its output.

A typical coal combustor operates with 20% excess air, has an inlet velocity on the order of 30 meters per second, and a coal inlet temperature close to room temperature. Combustor wall temperature ranges from 600 to 840 K, with a gas temperature of approximately 1400 K [8, 9, 12, 28, 29]. The residence time is about one second, and the typical coal will pass 80% by weight through a 75-μm screen.

For a base case, we use the values tabulated in Table 2. The relevant dimensionless parameters are the stoichiometric ratio, SR, the inlet diameter Reynolds number, Re_{D_c}, and the ratio of the combustor inlet diameter to the mass-mean diameter, D_c/D_{mm}. These are defined as

$$SR = \frac{\dot{m}_{\mathrm{air}} X_{\mathrm{O}_2}}{M_{\mathrm{O}_2}} \Bigg/ \frac{\dot{m}_{\mathrm{coal}}(1 - A_0)}{M_C} \tag{12}$$

and

$$\mathrm{Re}_{D_c} = \frac{D_c \bar{U}}{\nu}, \tag{13}$$

where

$$\bar{U} = \frac{\dot{m}_{\mathrm{air}} 4}{\rho \pi D_c^2}; \tag{14}$$

we use values of 1.2, 2×10^5, and 20.66 m/s, respectively, and D_c/D_{mm} is 40144. The important temperature ratios are the wall and gas temperatures divided by the coal inlet temperature. These are 3.5 and 1.75, respectively.

The particle-size distribution in pulverized coal is fairly well represented by the Rosin–Rammler distribution, where the mass

TABLE 2

Base Case for the Evaluation of Agglomeration Effects

Coal feed rate	5249 kg/h
Air feed rate	58000 kg/h
Gas temperature	1400 K
Wall temperature	700 K
Coal inlet temperature	400 K
Inlet diameter	2 m
Coal type	Anthracite
x' parameter	53 μm
n parameter	1.2
Number of fragments	1

fraction of particles exceeding a diameter D_p is given by the expression

$$R = \exp\left[-\left(D_p/x'\right)^n\right]. \quad (15)$$

Here x' is the size above which $1/e$ or 36.8% of the particles fall, and n is a measure of the size dispersion; the larger the n, the narrower the distribution. Typically, for a utility coal, $x' = 53$ μm and $n = 1.2$.

The mass mean diameter, D_{mm} can be found by integrating the product $D_p R(D_p)$ over D_p. This gives

$$D_{mm} = x'\Gamma\left(\frac{1}{n} + 1\right), \quad (16)$$

where Γ is the gamma function. For n between 1 and 1.5, $\Gamma(1/n + 1)$ varies between 1 and 0.9, indicating that x' is very close to D_{mm} for typical coals, and D_{mm} is 50 μm for the chosen grind.

In order to model agglomeration, the particle size distribution has been divided into bands. The mass fraction contained in a band is the difference between the edge values of the Rosin–Rammler distribution, $R(D_p)$, and is modeled as a constant diameter within the band. With the known diameter and mass fraction, the number density can be calculated from the relative flow rates for air and coal. Knowing the band number densities and diameters, the turbulent collision rate (Eqs. 5 and 6) between any two bands can be calculated, as can the collision rate for particles in a band colliding with each other. These rates are used to calculate the time derivatives of the number density and diameter in each band. For collisions involving two bands, the band with the smaller diameter will lose number density and mass, and the band with the larger diameter will gain mass. In the case of collisions within a band, there is only a change in number density. Combustion, however, will change only the diameter, not the number density.

These basic combustion equations apply to a pure carbon particle, unlike real particles which contain a non-combustible ash component. In order to simulate this ash content, the combustion rate is set to zero when the particle reaches the size of the sphere of ash that would remain after all the combustible matter has burned.

The combustion equations used assume that the only product of combustion is CO, which diffuses out from the particle to burn in the gas phase. Earlier research indicates this to be appropriate for pulverized fuels. To simplify the model, devolatilization products are assumed to burn away from the particle. These assumptions yield a tractable model, appropriate for iterative design, retrofitting work, and short computing cycles. In the interest of space, the details of the calculation are not included here, and the reader is referred to Ref. 33.

RESULTS

To interpret the results of this study, four parameters are important; $\bar{t}_b$, $t_{b0}/\bar{t}_b$, $(t_b/t_{b0}) - 1$, and $(dD_p/dt)_{combust}/(dD_p/dt)_{coag}$. Here, $\bar{t}_b$ is the characteristic time, t_{b0} is the burnout time without agglomeration, and t_b is the burnout time with agglomeration. The last term is the ratio of the rate of diameter decrease due to combustion to the increase in diameter due to agglomeration. The time $\bar{t}_b$ is found by assuming that a particle of the mass-mean diameter burns at constant density with an oxygen partial pressure of zero at its surface. The mass transfer equation for this is

$$q = \frac{4M_C \mathscr{D}_{O_2} P_g}{D_p R_g T_m}. \quad (17)$$

For a particle of constant density

$$\left(\frac{dD_p}{dt}\right)_{combust} = -\frac{2q}{\rho_p}. \quad (18)$$

Since T_m is difficult to define in this simple case, $(T_g + T_w)/2$ will be used instead. Hence,

$$\bar{t}_b = \frac{\rho_p R_g (T_g + T_w)}{32 M_C \mathscr{D}_{O_2} P_g} D_p^2. \quad (19)$$

which leads to $\bar{t}_b = 0.00656$ s for the base case. This is sufficiently close to that predicted by the more sophisticated model for 50-μm particles.

The ratio of the particle diameter change due to combustion to that due to agglomeration,

$$\left(\frac{dD_p}{dt}\right)_{\text{combust}} \Big/ \left(\frac{dD_p}{dt}\right)_{\text{coag}} = \left(\frac{2q}{\rho_p}\right) \Big/ \left(\frac{dD_p}{dt}\right)_{\text{coag}} = \frac{24 M_C P_g}{R_g \rho_p} \frac{\mathscr{D}_{O_2} \bar{t}_T}{D_p^2 T_m} e^{(-t/3\bar{t}_T)}, \tag{20}$$

is also an indicator of when agglomeration will be important. Substitution yields

$$\left(\frac{2q}{\rho_p}\right) \Big/ \left(\frac{dD_p}{dt}\right)_{\text{coag}} \cong \frac{T_m}{D_p^5 \eta_0} \sqrt{\frac{\nu D_c}{\bar{U}^3}}\, e^{(-t/3\bar{t}_T)}. \tag{21}$$

For the base case Eq. 21 reduces to

$$\left(\frac{2q}{\rho_p}\right) \Big/ \left(\frac{dD_p}{dt}\right)_{\text{coag}} = 382 e^{(-t/3\bar{t}_T)} \tag{22}$$

where $\bar{t}_T \approx 19$ h. Thus, when the right-hand side of Eq. 21 is on the order of unity (1 or 2 weeks), agglomeration is as important to change in particle diameter as combustion.

When the diameter history is normalized with respect to the initial diameter, all particle tracks collapse into one curve, as can be seen in Fig. 1. Closer examination of these curves at initial times in Fig. 2 reveals that agglomeration causes the particles to grow before they begin to burn. Furthermore, as shown in Fig. 3, the particles heat up to well over the equilibrium temperature during combustion, and then cool down to it as they burn out.

To verify the data on number density, the data on the largest particles were compared with those predicted by assuming a monodisperse suspension of these particles. The model and this theory differ by only 2%, and the theory does not account for diameter variations due to collisions with particles from the other bands.

The important results of this work are expressions predicting the burnout time with and without agglomeration, and the simulating code

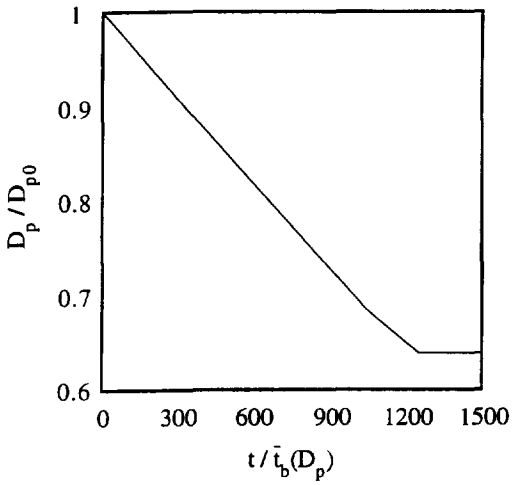

Fig. 1. Normalized diameter versus dimensionless time, illustrating the rate of particle-size reduction.

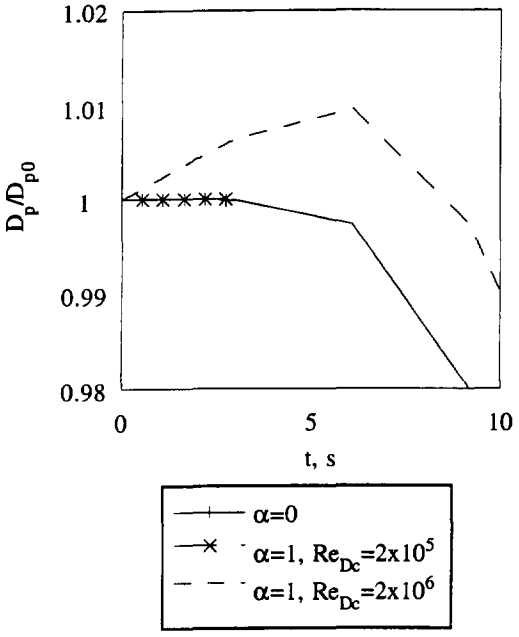

Fig. 2. Comparison between three turbulence levels.

itself. The burnout time without agglomeration is found by setting the collision efficiency to zero in the code, giving

$$\frac{t_{b0}}{\bar{t}_b} = 1.04 \times 10^{-9} \left(\frac{f^{1/3} D_c}{D_{\text{mm}}}\right)^2 \frac{T_g}{T_c} \left(7.21 - \frac{T_w}{T_c}\right). \tag{23}$$

By using the ratio of this to the burnout time it

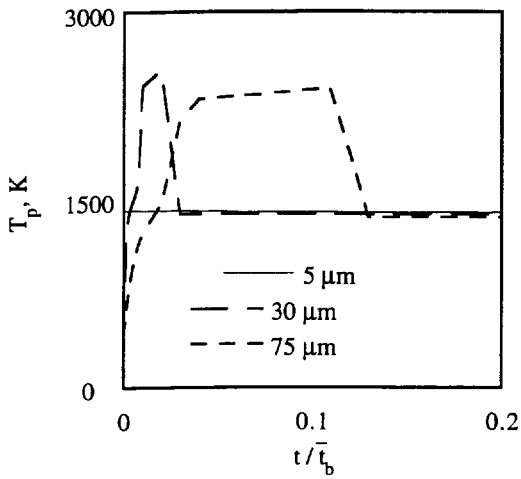

Fig. 3. Comparison of temperature histories for three initial particle sizes.

is possible to assess the added burnout time due to agglomeration:

$$\frac{t_b}{t_{b0}} = 1 + 2.03 \times 10^{-24} \frac{\alpha}{SR} \frac{T_g}{T_c} \mathrm{Re}_{D_c}{}^3 \times \left(8162 - \frac{f^{1/3} D_c}{D_{\mathrm{mm}}}\right). \quad (24)$$

This indicates when agglomeration can be expected to become important in combustor design, and will be valid for any reasonable combustor. Finally, using typical characteristics for utility coal combustors, agglomeration is predicted to become an important factor when Re_{D_c} exceeds about 2×10^6 or the combustion/agglomeration rate ratio is of order 1.

CONCLUSIONS

A model has been developed to study agglomeration during coal combustion. Results from this model provide a solid theoretical basis for the historical assumption that agglomeration can be ignored. Formulas have been developed to determine the range of conditions under which this assumption is valid. This range includes virtually all coal combustors.

The authors acknowledge the support of THECB / ERAP Grant no. 003604-014.

REFERENCES

1. Smoluchowski, M., *Z. Phys. Chem.* 92:129 (1917).
2. Gregory, J., *Crit. Rev. Environ. Control* 19:185–230 (1989).
3. Probstein, R. F., *Physicochemical Hydrodynamics*, Butterworths, Stoneham, MD, 1989.
4. Batchelor, G. K., *J. Fluid Mech.* 119:379–408 (1982).
5. Batchelor, G. K., *J. Fluid Mech.* 124:495–528 (1992).
6. Batchelor, G. K., *J. Fluid Mech.* 131:155–175 (1983).
7. Batchelor, G. K., *J. Fluid Mech.* 240:651–657 (1992).
8. Field, M. A., Gill, D. W., Morgan, B. B., and Hawksley, P. G. W., *Combustion of Pulverized Coal*, BUCRA, Leatherhead, 1967.
9. Jia, L., Becker, H. A., and Code, R. K., *International Conference on Fluidized Bed Combustion*, ASME, 1991, p. 1219.
10. Hill, S. C., and Smoot, L. D., *Ener. Fuels* 7:874–883 (1993).
11. Smith, P., and Smoot, L., *Coal Combustion and Gasification*, Plenum, New York, 1985.
12. Smoot, L., Pratt, D., *Pulverized Coal Combustion and Gasification*, Plenum, New York, 1979.
13. Singer, S., *Pulverized Coal Combustion*, Noyes, Park Ridge, NJ, 1984.
14. Baxter, L. L., *Combust. Flame* 90:199–209 (1992).
15. Kang, S., *Combust. Flame* 86:258–268 (1991).
16. Skryabin, A. A., and Belov, S. Yu., *Thermal Eng.* 39:432–435 (1992).
17. Walsh, P. M., Sarofim, A. F., and Beer, J. M., *Eng. Fuels* 6:709–715 (1992).
18. McCollor, D. P., Zygarlicke, C. J., Allan, S. E., and Benson, S. A., *Eng. Fuels* 7:761–767 (1993).
19. Cai, J., Lu, N., and Sorensen, C. M., *Langmuir* 9:2861–2867 (1993).
20. Sorensen, C. M., Cai, J., and Lu, N., *Appl. Opt.* 31:6547–6557 (1992).
21. Chang, H., and Biswas, P., *J. Colloid Interface Sci.* 153:157–166 (1992).
22. Puri, R., Richardson, T. F., and Santoro, R. J., *Combust. Flame* 92:222–320 (1993).
23. Probstein, R., Sonin, A., and Speilman, L., *Water Purification Present and Future Technology*, notebook.
24. Camp, T. R., and Stein, P. G., *J. Boston Soc. Civ. Eng.* 30:219 (1943).
25. Laufer, J., *U.S. Natl. Advis. Comm. Aeronaut.*, Rep. No. 1174 (1954).
26. Schlichting, H., *Boundary Layer Theory*, McGraw-Hill, New York, 1951.
27. Delichatsios, M. A., and Probstein, R. F., *J. Colloid Interface Sci.* 51:394 (1975).
28. Sanderson, D. K., and Germane, G. J., *Ener. Fuels* 7:910–918 (1993).
29. Bonin, M. P., and Queiroz, M., *Combust. Flame* 85:121–133 (1991).
30. Badzioch, S., Gregory, D. R., and Field, M. A., *Fuel* 43:267 (1964).
31. Baxter, L. L., *Combust. Flame* 90:174–184 (1992).
32. IMSL, Math/Library, IMSL Inc., Houston, 1991.
33. Shampine, R. W., Masters thesis, Rice University, 1994.

Received 9 December 1993; revised 25 July 1994

Erratum

This work was published in F. F. Grinstein and K. Kailasanath, *Comb. Flame* 100: 2–10 (1995), where Fig. 1 was inadvertently omitted. The full abstract of the paper, the missing figure, and minimal text discussing it are included here.

Three-Dimensional Numerical Simulations of Unsteady Reactive Square Jets

F. F. GRINSTEIN* and K. KAILASANATH

Laboratory for Computational Physics and Fluid Dynamics, Code 6410, U.S. Naval Research Laboratory, Washington, DC 20375-5844, USA

Results of finite-difference, time-dependent numerical studies of the near field of subsonic, reactive square jets were presented. The simulations model space/time-developing compressible (subsonic) jets, using species- and temperature-dependent diffusive transport, and finite-rate chemistry appropriate for H_2 combustion. Comparative measurements of entrainment for square jets were obtained based on evaluations of streamwise mass-flux to obtain an assessment on how the jet development is affected by chemical exothermicity and density differences between the jet and the surroundings. Depending on initial conditions (i.e., on the chemical exothermicity level implied by the initial reactant concentration), chemical energy release and expansion effects can be significant in determining reduced entrainment and initial jet growth relative to corresponding nonreactive jets. The instantaneous product formation rates are closely correlated with the local entrainment rates controlled by the vorticity bearing fluid. Instantaneous entrainment rates—based on the rate of increase of mass flux of rotational fluid—were found to be significant in the regions of roll-up and initial self-deformation of vortex rings, and then farther downstream, in the vortex merging region, where fluid and momentum transport between the jet and its surroundings are considerably enhanced by the presence of hairpin vortices aligned with the corners. Analysis of the combustion dynamics in terms of scalar mixing fraction diagnostics previously used in laboratory reactive turbulent jet experiments, was shown to be also potentially useful in characterizing their transitional regime by bringing out the relation between product formation rates and underlying fluid dynamical events.

DISCUSSION

Figure 1 exemplifies the unsteady jet dynamics for "Run 5" from [1], at two typical times, in terms of volume renderings of the temperature, vorticity magnitude, and fuel molar fraction. The dynamics of non-reactive square jets has been discussed elsewhere [2]. Specific combustion features of the reactive jet development—some of which are illustrated in Fig. 1—include: 1) more disorganized vorticity dynamics in the reactive jets due to expansion effects and baroclinic vorticity production associated with chemical exothermicity; 2) distinct high-temperature regions associated with the convective concentration of burnt gas—mainly composed of product and diluent—and governed by the dynamics of vortex-ring deformation and hairpin (braid) vortices; and 3) instantaneous chemical production occurring at the outer edges of the rings, in the high-strain neighborhoods of the interfaces between reactants, where diffusive mixing takes place for the relatively fast flows considered here [3].

REFERENCES

1. Grinstein, F. F., Kailasanath, K., *Comb. Flame* 100: 2–10 (1995).
2. Grinstein, F. F., Gutmark, E., and Parr, T., *Phys. Fluids* (June, 1995), to appear.
3. Grinstein, F. F., and Kailasanath, K., *Phys. Fluids A* 4:2207(1992).

*Corresponding Author. Presented at The Twenty-fifth Symposium (International) on Combustion, Irvine, CA, July 31–August 5, 1994.

0010-2180/95/$9.50
SSDI 0010-2180(95)00062-B

COMBUSTION AND FLAME 101:192 (1995)

Published by Elsevier Science Inc.

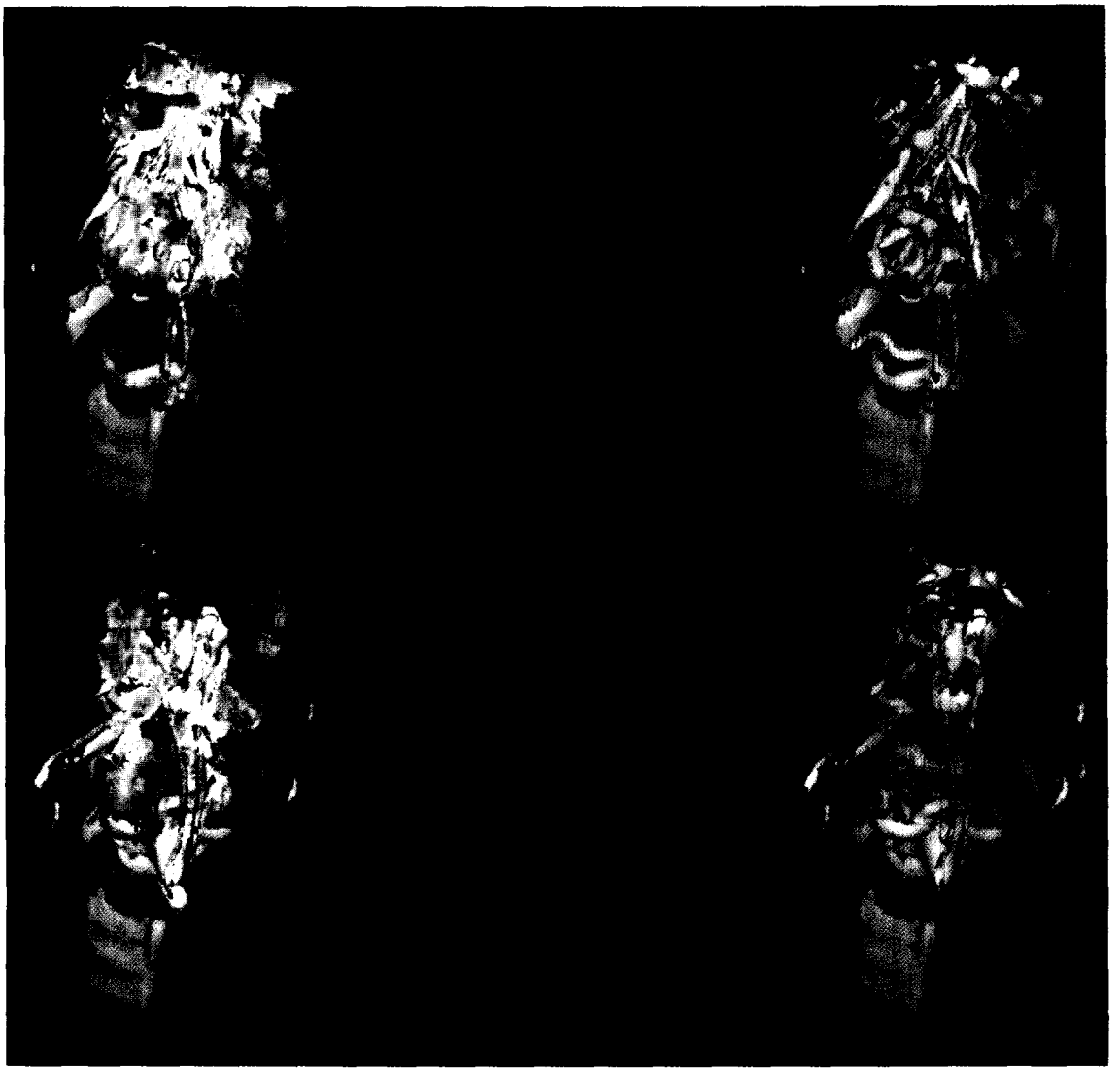

Fig. 1. Unsteady jet dynamics for Run 5 at two typical times, in terms of (color) volume renderings of temperature (a), vorticity magnitude (b) and fuel molar fraction (c), ranging between minimum (semi-transparent blue) and maximum (opaque red) values: (a) T_o–$1.8T_o$, (b) $0.1\Omega_{peak}$–Ω_{peak}, (c) 0.0–0.4. Isosurfaces (gray-shaded) of the vorticity magnitude (Ω) for $\Omega = 0.5\Omega_{peak}$ have been superimposed for reference in frames a) and c) . The flow direction is from bottom to top in each frame, and time advances from the top to the bottom row (time separation is $\tau = 1/f$).